Radiation Physics and Chemistry 203 (2023) 110594

Contents lists available at ScienceDirect

Radiation Physics and Chemistry

journal homepage: www.elsevier.com/locate/radphyschem

K- and L-shell theoretical fluorescence yields for the Fe isonuclear sequence

Daniel Pinheiro [a,*], André Fernandes [a], César Godinho [a], Jorge Machado [a,*], Gonçalo Baptista [a], Filipe Grilo [a], Luís Sustelo [a], Jorge M. Sampaio [b], Pedro Amaro [a], Roberta G. Leitão [a], José P. Marques [b,c], Fernando Parente [a], Paul Indelicato [d], Miguel de Avillez [e,f], José Paulo Santos [a], Mauro Guerra [a]

[a] Laboratory of Instrumentation, Biomedical Engineering and Radiation Physics (LIBPhys-UNL), Department of Physics, NOVA School of Science and Technology, NOVA University Lisbon, 2829-516 Caparica, Portugal
[b] LIP-Laboratório de Instrumentação e Física Experimental de Partículas, Avenida Professor Gama Pinto 2, 1649-003 Lisboa, Portugal
[c] Faculdade de Ciências da Universidade de Lisboa, Campo Grande 016, 1749-016 Lisboa, Portugal
[d] Laboratoire Kastler Brossel, Sorbonne Université, CNRS, ENS-PSL Research University, Collège de France, Case 74; 4, place Jussieu, F-75005 Paris, France
[e] Computational Astrophysics Group, Institute for Research and Advanced Training, University of Évora, R. Romão Ramalho 59, 7000-761 Évora, Portugal
[f] Zentrum für Astronomie und Astrophysik, Technische Universität Berlin, Hardenbergstrasse 36, 10623 Berlin, Germany

ARTICLE INFO

Keywords:
Fundamental parameters
Fluorescence yield
Atomic data
K-shell
L-shell

ABSTRACT

In this work, we present K- and L- shell fluorescence yield values of the full isonuclear sequence of Fe ions, using a state-of-the-art multiconfiguration Dirac–Fock approach. These results may be of importance for spectral fitting and plasma modeling, both in laboratory and astrophysical studies, where Fe is an important benchmark element. The K-shell fluorescence yields were found to be very similar up to the removal of 14 electrons.

1. Introduction

In order to extract meaningful information from physical systems through X-ray emission or absorption spectra, some aspects of atomic data are required such as line energies and widths, transition rates, mass attenuation coefficients and fluorescence yields, just to name a few. This is true for X-ray emission of bulk, solid materials as well as liquids, gases and plasmas (Grieken and Markowicz, 2002). Given the wide interest of X-ray techniques in both academia and industry, there are extensive databases with the relevant atomic parameters for elemental quantification of almost every element in the periodic table (Bambynek et al., 1972; Krause and Oliver, 1979; Hubbell et al., 1994; Schoonjans et al., 2011). These parameters, however, feature high relative uncertainties, especially in the low energy regime, and are mostly confined to neutral elements. In fact, when trying to characterize nanostructured materials, given the lack of standard reference samples, there is no other way than to rely on precise X-ray fundamental parameters, together with calibrated instrumentation, to reliably correlate material functionalities with their underlying chemical and physical properties, through their emission spectra (Kolbe et al., 2005). Measurement and calculation of these atomic parameters with low uncertainties, are the main goal of the International Initiative on X-ray Fundamental Parameters (IIFP), a collaboration between world class metrology institutes, universities, and key enterprises operating in the X-ray spectroscopy market (Initiative, 2017). Among the parameters of interest for the IIFP is the Fluorescence Yield (FY), which describes how an ionized atom, with a hole in any given shell will relax to another lower energy configuration, either by emitting an X-ray photon or through the emission of an Auger electron. This is one of the key parameters in order to extract information on the abundance of a given element or ion in any physical medium, since it relates the number of atoms with holes in a given shell and the number of emitted X-rays from the decay of these one-hole states (Liu et al., 2014; Kolbe et al., 2012). This is especially important when trying to derive elemental abundances from astrophysical plasmas using either ground based or spatial observatories (Liu et al., 2014). Given that the temperature of astrophysical plasmas drives the ionization rates and thus the charge state distribution, one needs a copious amount of atomic physics data when trying to perform spectral fitting or collisional radiative modeling of these objects (de Avillez et al., 2019).

Although extensive tables of FY for all values of Z exist in literature, they are insufficient for several applications, both experimental and theoretical. In many instances, several charge states will contribute to the final emission spectra, due to shake, ionization, and radiationless transition processes, which need to be taken into account for a full

* Corresponding authors.
E-mail addresses: ds.pinheiro@campus.fct.unl.pt (D. Pinheiro), jfd.machado@fct.unl.pt (J. Machado).

https://doi.org/10.1016/j.radphyschem.2022.110594
Received 22 March 2022; Accepted 9 October 2022
Available online 14 October 2022

description. Furthermore, previous works have shown that significant changes in the FY of different shells can be observed for different charge states of the same atomic system (Larkins, 1971; Marques et al., 2020). Motivated by Larkins et al. work (Larkins, 1971), Fortner and coworkers (Fortner et al., 1972) studied the changes of the copper L-shell FY as a function of the number of M-shell electrons in the initial configuration, and did not find a behavior similar to the one found by Larkins for Argon ions. In fact, the FY value remained fairly constant up to the removal of six of the outer shell electrons. Arndt and Hartmann (1983) calculated the K-shell fluorescence yield for highly charged lead ions, showing that the K-shell FY value is almost unaffected by the removal of outer-shell electrons. On the other hand, Phillips et al. (1987) performed new measurements of the fluorescence yields of inner shell electrons in highly stripped ^{57}Fe ions, and found large variations of these values with the charge state. Regarding the calculations made for multiply-stripped hollow neon atoms with double K-shell vacancies by Karim and Logan, Karim and Logan (1999) using the Hartree–Fock model, the FY were found to decrease as the electron population in the outer L-shell increases. For the isoelectronic series of Ne, Ar and Kr, Marques et al. shown that although the K FY almost does not change with the nuclear charge, when compared to the neutral atom's FY, the same is not true for the L-shell, showing very large variations (Marques et al., 2020).

There are several databases of atomic parameters that are widely used in astrophysics (Smith et al., 2001; Foster et al., 2013; Kaastra and Mewe, 1993; Dere et al., 1997; Kallman and Palmeri, 2007), and they also have their own strengths and weaknesses, one of the latter being the fact that the atomic physics approximations used in the calculation of these parameters are much more realistic for isolated atoms in plasmas than in solid state materials. There are, however, some issues even with the most widely used databases, as shown for example by Gorczyca et al. (2003). In their work, they audited the fluorescence database by Kaastra and Mewe (1993), which is widely used in modeling codes, in particular their scaling laws along isoelectronic sequences. They found serious discrepancies that seem to hinder its application in plasma modeling.

The inclusion of different charge states in the simulations is particularly important in the case of plasma and astrophysical studies, as various diagnostics are performed based on the emitted X-ray radiation from the plasma or astrophysical object in study (Guerra et al., 2013). Various features can be determined from the X-ray spectra of galaxies, and one of the important elements to measure in the spectra is Fe, particularly the Fe K line energy, width, shape and relative intensity. This metal presence and abundance can give information about the astronomical system, for example on the presence and composition of the torus around active galactic nuclei (Fukazawa et al., 2016).

As shown in many recent publications, the precise calculation of these parameters requires state of the art methods such as the Multi-Configuration Dirac–Fock (MCDF) method and for all but the simplest open shell configurations, this task is quite demanding in terms of CPU time and resources (Cheung et al., 2021; Guerra et al., 2018, 2015). A distributed computation script that enables the use of supercomputers with a near-perfect linear scalability with the number of cores, was developed based on gnu Parallel shell tool (Tange, 2018) to compute wavefunctions and transition rates within the MCDF framework.

In this work, we calculate the energies and wavefunctions for every one- and two-hole levels, transition probabilities and widths for all possible radiative and radiationless transitions of the complete Fe isonuclear sequence, using the multiconfiguration Dirac–Fock General Matrix Elements (MCDFGME) code developed by Desclaux and Indelicato. From these values, the fluorescence yield of each of the Fe subshells was obtained.

2. Theory

2.1. MCDF

Following previous works (e.g. Guerra et al. (2021)) all the transition energies, radiative and radiationless rates necessary to evaluate the FY of each subshell were obtained from calculations, employing the state-of-the-art multiconfiguration Dirac–Fock (MCDF) method. In this method, the atomic antisymmetric wave function ψ is written as a linear combination of the φ configuration state functions (CSF): $\psi(1, 2, \ldots, N) = \sum_i a_i \varphi_i$, where a_i are mixing coefficients. In this way the electronic correlation is included.

The relativistic general purpose multiconfiguration Dirac–Fock code (MCDFGME) developed by J. P. Desclaux, P. Indelicato and co-authors (Desclaux, 1975; Indelicato and Desclaux, 1990; Indelicato et al., 2007; Santos et al., 2005) implements the MCDF method, using a self-consistent field approach. The self-consistent field calculation includes various contributions, such as Coulomb and Breit (magnetic and retardation parts), both containing direct and exchange components, as well as quantum electrodynamics (QED) local potentials, such as vacuum polarization. Other QED contributions, such as self-energy, are also included as perturbations.

For the calculation of radiative rates, the optimized-level method was used to calculate the wave functions and energies of both the initial and final states, considering full relaxation. As each state was optimized separately, they are not necessarily orthogonal and, to calculate radiative rates, the formalism described by Löwdin (1955) was used. Moreover, the length gauge was considered for all radiative transition rates. In the case of radiationless rates, the continuum-electron wavefunctions are obtained by solving the Dirac–Fock equations with the same atomic potential of the initial state. Here, no relaxation was allowed in both initial and final states of the radiationless process.

2.2. Decay rates, subshell widths, and fluorescence yields

The fluorescence yield of an atomic subshell is defined as

$$\omega_i = \frac{\Gamma_i^R}{\Gamma_i^R + \Gamma_i^{NR}}, \tag{1}$$

where Γ_i^R and Γ_i^{NR} are, respectively, the radiative and radiationless widths of a one-hole subshell i. The width of a subshell i is given by the sum of partial widths Γ_{ij} of all the possible decay paths. In the case of radiative transitions the width is defined as

$$\Gamma_i^R = \sum_j \Gamma_{ij}^R, \tag{2}$$

where j represents a subshell with lower energy than the ith subshell. For the case of radiationless transitions the width is defined similarly taking into account the creation of a second hole in the subshell k

$$\Gamma_i^{NR} = \sum_j \sum_k \Gamma_{ij;k}^{NR}, \tag{3}$$

where k represents a subshell with higher or equal quantum numbers to the subshell j. In the case of the k subshell being equal to the j subshell we have a Coster–Kronig transition, otherwise we have an Auger transition ($k > j$).

3. Results and discussion

In this work we calculated the complete set of possible radiative and radiationless transitions of the Fe isonuclear sequence using the state-of-the-art MCDFGME code. A table with the initial electronic configurations of each Fe ion, considered for this calculation, can be found in Table 1. These configurations reflect the ground state of the Fe isonuclear sequence, and were taken from Rodrigues et al. (2004). The necessary 1-hole and 2-hole configurations, and the resulting levels, were obtained from these.

Table 1
Initial electronic configurations for each Fe ion, obtained from Rodrigues et al. (2004).

Fe ion (Charge State)	Configuration
Fe I (0+)	$[Ar]3d^6 4s^2$
Fe II (1+)	$[Ar]3d^6 4s^1$
Fe III (2+)	$[Ar]3d^6$
Fe IV (3+)	$[Ar]3d^5$
Fe V (4+)	$[Ar]3d^4$
Fe VI (5+)	$[Ar]3d^3$
Fe VII (6+)	$[Ar]3d^2$
Fe VIII (7+)	$[Ar]3d^1$
Fe IX (8+)	$[Ne]3s^2 3p^6$
Fe X (9+)	$[Ne]3s^2 3p^5$
Fe XI (10+)	$[Ne]3s^2 3p^4$
Fe XII (11+)	$[Ne]3s^2 3p^3$
Fe XIII (12+)	$[Ne]3s^2 3p^2$
Fe XIV (13+)	$[Ne]3s^2 3p^1$
Fe XV (14+)	$[Ne]3s^2$
Fe XVI (15+)	$[Ne]3s^1$
Fe XVII (16+)	$1s^2 2s^2 2p^6$
Fe XVIII (17+)	$1s^2 2s^2 2p^5$
Fe XIX (18+)	$1s^2 2s^2 2p^4$
Fe XX (19+)	$1s^2 2s^2 2p^3$
Fe XXI (20+)	$1s^2 2s^2 2p^2$
Fe XXII (21+)	$1s^2 2s^2 2p^1$
Fe XXIII (22+)	$1s^2 2s^2$

Table 2
Number of transitions computed as a function of the Fe ion charge state. The values are presented as the number of radiative + radiationless transitions.

Charge State	# of transitions	Charge State	# of transitions
0+	210 276+951 621	12+	1081+1769
1+	726 614+2 759 303	13+	253+330
2+	171 404+628 699	14+	10+20
3+	233 586+755 189	15+	36+38
4+	161 028+493 451	16+	6+10
5+	58 653+168 105	17+	78+60
6+	9730+28 583	18+	210+160
7+	666+1780	19+	300+150
8+	21+70	20+	153+80
9+	351+650	21+	36+12
10+	1224+2292	22+	1+1
11+	1953+2963		
Total	6 821 008		

This isonuclear sequence has a great interest in astrophysics, particularly the fluorescence yield of each charge state. Frequently, in several applications, and given the difficulty in calculating the fluorescence yields for each electronic configuration of interest, the FY of various charge states is approximated by its value for the neutral atom.

In Table 2 the total number of transitions (radiative + radiationless) that were computed in this work is shown, as a function of the charge state of the Fe ion.

From the calculated transition rates in the length gauge and using Eq. (1) we show the variation of the fluorescence yield for the K-, L_1-, L_2- and L_3-shells along the isonuclear sequence. These variations are compared with the reference values from Krause (1979) and XRayLib (Sánchez Del Río et al., 2003) for the neutral Fe atom, starting with the K-shell in Fig. 1.

The variation of the number of electrons not only changes the number of possible combinations for both radiative and radiationless transitions, but it also modifies the energy eigenvalues of the states corresponding to the various orbitals. These changes can result in the opening or closing of radiative and/or Auger channels that are otherwise, respectively, closed or open in the neutral atom. The FY of each occupied subshell of the atom or ion would then change, as the FY depends on the sum of the transition rates for all possible final states from any initial state in that subshell. The FY values of all the charge states of Fe up to Fe XXIII (C.S. 22+) are presented in Table 3. As can

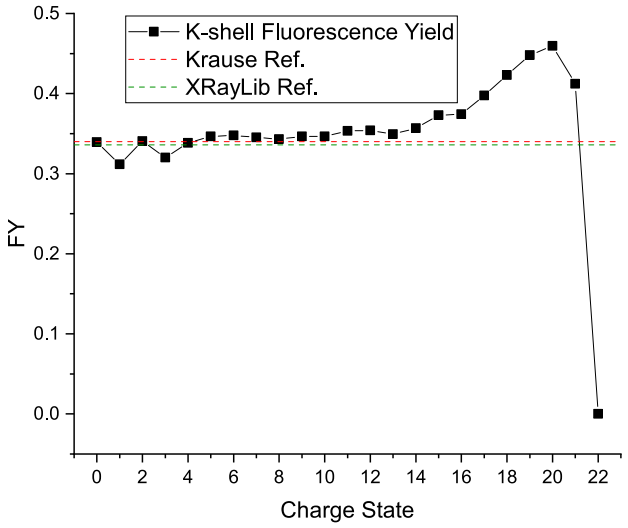

Fig. 1. Variation of the K-shell fluorescence yield with charge state in the Fe isonuclear sequence.

Table 3
Calculated K-shell FY values for the Fe isonuclear sequence.

Charge State	K-shell FY	Charge State	K-shell FY
0+	0.339	12+	0.354
1+	0.312	13+	0.349
2+	0.341	14+	0.357
3+	0.320	15+	0.373
4+	0.338	16+	0.374
5+	0.347	17+	0.397
6+	0.348	18+	0.423
7+	0.345	19+	0.448
8+	0.343	20+	0.460
9+	0.347	21+	0.412
10+	0.347	22+	2.62×10^{-6}
11+	0.353		

be seen, small fluctuations of the order of 0.01 (less than 10%), are observed in the K-shell FY from the ground state up until the Fe^{14+} (Fe XV). This result points in the direction of the findings of Larkins (1971) for the L-shell of Cu, where they found very small changes in the FY up to the removal of the outer six electrons. It also mimics the results from Marques et al. where the K-shell FY of Ne, Ar and Kr isoelectronic sequences seem to be insensitive to the nuclear charge Z (Marques et al., 2020). A more significant variation of the FY can be observed in the remaining charge states (Fe^{15+} to Fe^{21+}), with a FY value that peaks for Fe^{20+} of 0.460. This FY value is more than 35% higher than its counterpart for the neutral Fe. Since in the present framework, the Be-like Fe^{22+}, with a K-hole, can only decay through a M1 transition, $1s2s^2\ {}^2S_{1/2} \longrightarrow 1s^2 2s\ {}^2S_{1/2}$, or by emitting an Auger electron, $1s2s^2\ {}^2S_{1/2} \longrightarrow 1s^2\ {}^1S_0$, with a transition rate that is 6 orders of magnitude higher, its corresponding FY should be very close to zero, as observed in our calculations. In fact, for this particular ion, the main radiative channel corresponds to the two-electron one-photon transition $1s2s^2\ {}^2S_{1/2} \longrightarrow 1s^2 2p\ {}^2P_{1/2}$ with an E1 transition rate of $7.85 \times 10^{+8}\ s^{-1}$, 2.5 times higher than the M1 transition with a rate of $3.05 \times 10^{+8}\ s^{-1}$. This would increase the K-shell FY of Fe^{22+} to 6.74×10^{-6} instead of the 2.62×10^{-6} presented in Table 3.

This behavior is expected as the number of Auger channels decreases quicker than the number of radiative transitions when the shell above the one for which the FY is being computed, starts to have its electrons removed. Between Fe^{14+}, where the $3s$ orbital is fully occupied and Fe^{15+}, where the $3s$ orbital contains only one electron, we observe a change in FY of approximately 0.02 (10% compared to

Table 4
Calculated L_1-shell FY values from the MCDFGME code for the Fe isonuclear sequence.

Charge State	L_1-shell FY	Charge State	L_1-shell FY
0+	0.000599	11+	0.0136
1+	0.000647	12+	0.0124
2+	0.000712	13+	0.00967
3+	0.000959	14+	0.00186
4+	0.00159	15+	1
5+	0.00231	16+	1
6+	0.0117	17+	1
7+	0.0150	18+	1
8+	0.0149	19+	1
9+	0.0145	20+	1
10+	0.0142	21+	1

the neutral atom's FY) due to the opening of mostly radiative transition channels. This can be easily seen in Table 2. From Fe^{14+} to Fe^{15+} there was an increase of 26 radiative channels compared to 18 radiationless channels. Additionally, the charge states 15+ and above are dominated by radiative transition channels, up to 3 times more radiative channels than radiationless channels for charge state 21+. Although we observe a larger number of radiative channels for charge states 15+ and above, the FY is always smaller than 0.5. This is due to the fact that the radiationless rates for these ions have much higher rates than the radiative ones.

Additionally, a similar change of 0.02 (10%) in the FY is observed between Fe^{2+} and Fe^{3+} due to the fact that the ground state configuration for Fe III (2+) is $[Ar]3d^5 4s^1$ while for Fe IV (3+) we have $[Ar]3d^3 4s^2$, leading to an increase in the number of possible terms and thus radiative and Auger transitions. Although the number of both radiative and radiationless transitions are higher than their counterpart for Fe^{2+}, the radiative yield decreases slightly while the radiationless yield remains fairly constant. A similar behavior is also observed between Fe^{0+} and Fe^{1+}.

We also present the results for the L_1-, L_2- and L_3-shells calculated within the same theoretical framework in Tables 4–6 respectively.

As can be seen in Tables 4–6, the calculated FY for charge states higher than Fe^{14+} is exactly 1 due to the lack of electrons occupying higher energy orbitals making radiationless transitions impossible. Also, for Fe^{22+} there are no electrons in the $2p$ orbital, i.e. there is no possible radiative (or radiationless) transitions to the L_1 shell, and for Fe^{21+} with a configuration $1s^2 2s^2 2p$ there are no possible transitions with an initial hole in the $L_{2,3}$ shell. The first interesting conclusion one can draw, from the results of the L-subshells, is that the behavior of the L_1-subshell FY as a function of the charge state is drastically different from the $L_{2,3}$ subshells. At first sight, the rise of the L_2 and L_3 FY values, from Fe^{12+} forward, is easily explained since the number of Auger channels decrease rapidly as the number of $3p$ electrons are removed. This, however, does not explain the results for the L_1 subshell. This peculiar variation of the FY is explained by a combination of factors, which includes the weight of the L_1-$M_{4,5}M_{4,5}$ and the L_1-$M_{4,5}$ transitions in the L_1 radiationless and radiative widths, respectively. The quick rise of the L_1 FY from Fe^{5+} ($[Ar]3d^3$) to Fe^{6+} ($[Ar]3d^2$), reflects the change in the L_1-$M_{4,5}M_{4,5}$ partial widths, which are 0.34 eV and 0.05 eV for Fe^{5+} and Fe^{6+}, respectively (for Fe^{7+} this partial width is 0 since there is only one $3d$ electron). These partial widths should also be compared to the total radiative and radiationless widths of Fe^{5+} and Fe^{6+}. For Fe^{5+}, the L_1 Auger width of 57.27 eV is about two orders of magnitude higher than the partial width of the L_1-$M_{4,5}M_{4,5}$ transitions, which in turn is about twice the radiative L_1 width of 0.13 eV. For Fe^{6+} the L_1-$M_{4,5}M_{4,5}$ partial width of 0.05 eV is about two orders of magnitude lower than the L_1 Auger width of 4.96 eV (similar to Fe^{5+}), but is almost the same as its radiative width of 0.06 eV. This means that the L_1-$M_{4,5}M_{4,5}$ transition rates have a similar weight in the L_1 Auger width for both charge states, but for Fe^{6+} it features a weight,

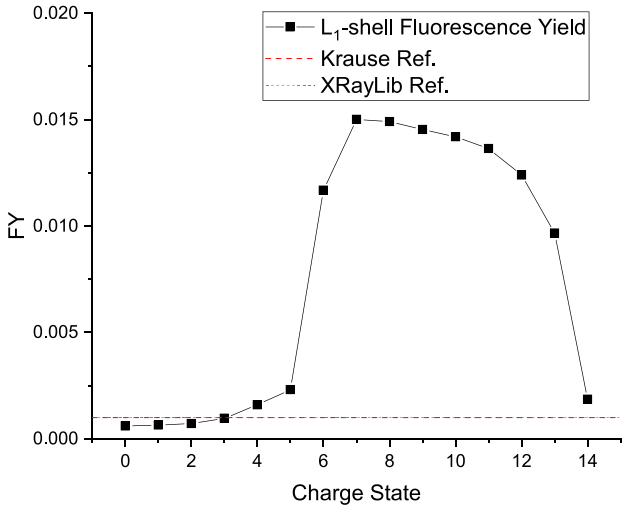

Fig. 2. Variation of the L_1-shell fluorescence yield from neutral Fe to Fe^{14+}.

Table 5
Calculated L_2-shell FY values from the MCDFGME code for the Fe isonuclear sequence.

Charge State	L_2-shell FY	Charge State	L_2-shell FY
0+	0.00642	11+	0.00206
1+	0.00661	12+	0.00585
2+	0.00656	13+	0.0154
3+	0.00685	14+	0.0902
4+	0.00707	15+	1
5+	0.00681	16+	1
6+	0.00579	17+	1
7+	0.00363	18+	1
8+	0.000749	19+	1
9+	0.00236	20+	1
10+	0.000786		

relative to the radiative transition rates, that is much less pronounced. In the end this will result as a much higher fluorescence yield. The same is true going from Fe^{6+} to Fe^{7+}, where the weight of the L_1-$M_{4,5}M_{4,5}$ partial width is zero. The decrease in the FY from Fe^{7+} to Fe^{14+} is due to the number of $2s \longrightarrow 3p$ transitions that decreases faster than the number of L_1-$XM_{2,3}$ (X = $L_{2,3}$, M1 and $M_{2,3}$) transitions. This apparent counterintuitive explanation seems not to represent what is seen in the L_2 and L_3 FY, since the closing of the $L_{2,3}$-$M_{4,5}M_{4,5}$ Auger channels also start to dominate at the Fe^{6+} ion. What changes from the L_1 case is that, although the radiative width of the $L_{2,3}$ subshells are very similar to the L_1 case, almost all of the width comes from the $2p \longrightarrow 3d$ radiative transitions, whereas for L_1 it comes essentially from $2s \longrightarrow 3p$ transitions. Thus, the influence of removing the $3d$ electrons will change both the radiative and radiationless widths in a similar fashion for the $L_{2,3}$ FY, leaving it unchanged. This is not true for the L_1 FY since the radiative rate is dominated by $2s \longrightarrow 3p$ transitions but the radiationless transitions are much more sensitive to the removal of the $3d$ electrons (see Fig. 2).

For the same reasons as mentioned before, the L_2- and L_3-shells FY behavior from Fe^{15+} to Fe^{20+} is equal to the L_1-shell FY, i.e. a radiationless yield of 0. However, for both the L_2- and L_3-shells the FY maximum (excluding the cases where FY = 1) corresponds to Fe^{14+} where the $3s$ orbital is completely filled (see Figs. 3 and 4). For Fe^{15+}, the $3s$ orbital only has one electron, resulting in no possible radiationless transitions to the $2p$ orbital. In the case of Fe^{13+} the $3p$ orbital also has one electron resulting in an increase of radiationless yield compared to Fe^{14+}.

Another interesting case is the FY minimum, for Fe^{8+}, where the $3p$ orbital is filled, resulting in a decrease of number of transitions

Table 6
Calculated L_3-shell FY values from the MCDFGME code for the Fe isonuclear sequence.

Charge State	L_3-shell FY	Charge State	L_3-shell FY
0+	0.00456	11+	0.00587
1+	0.00440	12+	0.0149
2+	0.00458	13+	0.0587
3+	0.00399	14+	0.0946
4+	0.00342	15+	1
5+	0.00271	16+	–
6+	0.00211	17+	1
7+	0.00149	18+	1
8+	0.000751	19+	1
9+	0.00491	20+	–
10+	0.00659		

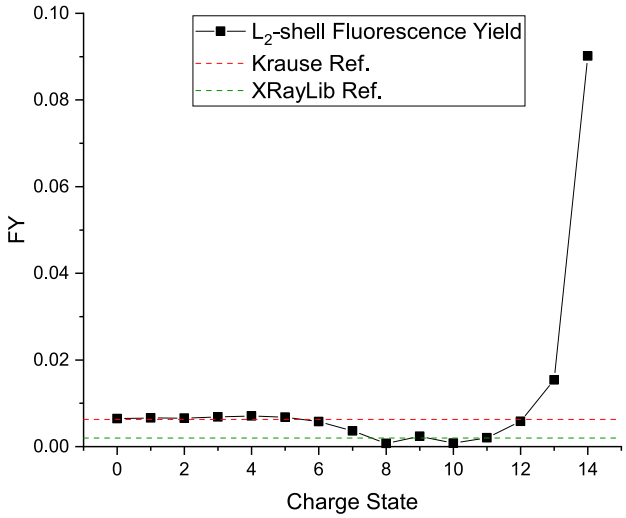

Fig. 3. Variation of the L_2-shell fluorescence yield from neutral Fe to Fe^{14+}.

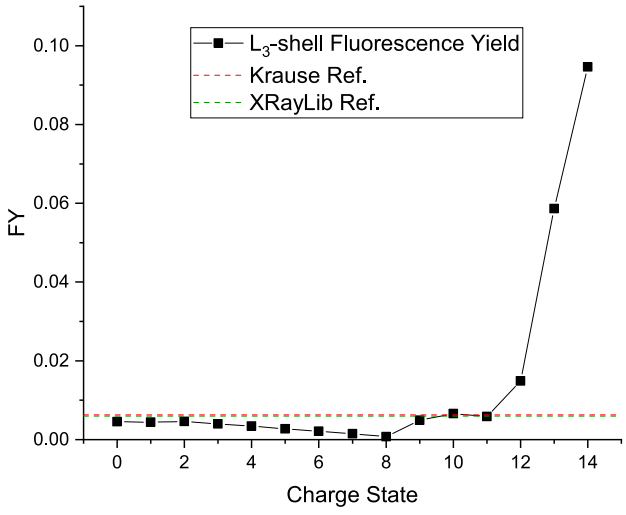

Fig. 4. Variation of the L_3-shell fluorescence yield from neutral Fe to Fe^{14+}.

(Table 2). Although, as explained before, both the radiative and radiationless yields decrease due to the lower number of both types of transitions, the radiative yield has a greater drop than the radiationless yield. As expected, this is observed for both the L_2- and L_3-shells.

4. Conclusion

In this work we have calculated a large set of level energies and transition rates, both radiative and radiationless, for the Fe isonuclear sequence. These calculations were performed using the multiconfiguration Dirac–Fock formalism in the monoconfiguration framework. Since the calculated levels are obtained in the LS coupling scheme, whereas they are calculated in the jj scheme, a small amount of electron correlation is naturally included in all calculations. Given the enormous amount of transitions that had to be computed in this work, around 7 million, an in-house code was built making use of standard parallelization tools. The K- and L-shell fluorescence yields of all the Fe isonuclear sequence were computed for the first time from first principles showing for the K-shell that the removal of the valence electrons results in a very small variation of the FY. For the L-shell the behavior was quite different from the one observed in other works for Cu ions where the average L-shell fluorescence yield was found to be very similar up to the removal of six M-shell electrons. For the $L_{2,3}$ FY this seems to be the case, but not for the L_1 FY where a sharp rise of the FY is found around Fe^{5+} to Fe^{7+} and a subsequent decrease from Fe^{12+} to Fe^{14+}. This variation is explained by the different influence of the removal of the last three $3d$ electrons on the relative radiationless partial widths when compared to the radiative widths, which change very differently for the L_1 and $L_{2,3}$ cases due to the radiative selection rules.

Declaration of competing interest

The authors declare that they have no known competing financial interests or personal relationships that could have appeared to influence the work reported in this paper.

Acknowledgments

This research was funded in part by FCT (Portugal) under research center grant UID/FIS/04559/2020 (LIBPhys). This work was also funded through the project PTDC/FIS-AQM/31969/2017, "Ultra-high-accuracy X-ray spectroscopy of transition metal oxides and rare earths". F.G. acknowledges support from FCT, Portugal through contract UI/BD/151000/2021. J. M and J.P.S acknowledge the support of EMPIR, Germany, under Contract No. 20FUN04 PrimA-LTD. The EMPIR initiative is co-funded by the European Union's Horizon 2020 research and innovation programme and the EMPIR, Germany participating States. Part of this work has been carried out under the High Performance Computing Chair - a R&D infrastructure (based at the University of Évora; PI: M. Avillez), endorsed by Hewlett Packard Enterprise (HPE), and involving a consortium of higher education institutions (University of Algarve, University of Évora, NOVA University Lisbon, and University of Porto), research centres (CIAC, CIDEHUS, CHRC), enterprises (HPE, ANIET, ASSIMAGRA, Cluster Portugal Mineral Resources, DECSIS, FastCompChem, GeoSense, GEOtek, Health Tech, Starkdata), and public/private organizations (Alentejo Tourism-ERT, KIPT Colab).

References

Arndt, E., Hartmann, E., 1983. Deexcitation rates and fluorescence yields of highly stripped atoms. Phys. Lett. A 95 (3), 146–147.

Bambynek, W., Crasemann, B., Fink, R.W., Freund, H.U., Mark, H., Swift, C.D., Price, R.E., Rao, P.V., 1972. X-Ray fluorescence yields, auger, and coster-kronig transition probabilities. Rev. Modern Phys. 44 (4), 716–813. http://dx.doi.org/10.1103/RevModPhys.44.716.

Cheung, C., Safronova, M., Porsev, S., 2021. Scalable codes for precision calculations of properties of complex atomic systems. Symmetry 13 (4), 621.

de Avillez, M.A., Guerra, M., Santos, J.P., Breitschwerdt, D., 2019. Relativistic electron impact ionization cross sections of carbon ions and application to an optically thin plasma. Astron. Astrophys. 631, A42. http://dx.doi.org/10.1051/0004-6361/201935337.

Dere, K.P., Landi, E., Mason, H.E., Fossi, B.C.M., Young, P.R., 1997. CHIANTI - an atomic database for emission lines. Astron. Astrophys. Suppl. Ser. 125 (1), 149–173.

Desclaux, J.P., 1975. A multiconfiguration relativistic DIRAC-FOCK program. Comput. Phys. Comm. 9 (1), 31–45. http://dx.doi.org/10.1016/0010-4655(75)90054-5.

Fortner, R.J., Der, R.C., Kavanagh, T.M., Garcia, J.D., 1972. Variation of copper L shell fluorescence yield in ion-atom collisions. J. Phys. B: Atom. Mol. Phys. 5 (4), L73–L75.

Foster, A.R., Ji, L., Yamaguchi, H., Smith, R.K., Brickhouse, N.S., 2013. AtomDB: Atomic data for X-ray astronomy. AIP Conf. Proc. 1545 (1), 252–259.

Fukazawa, Y., Furui, S., Hayashi, K., Ohno, M., Hiragi, K., Noda, H., 2016. Fe–K line time variability an Ni abundance of distant reflectors in seyfert galaxies. Astrophys. J. 821 (1), 15. http://dx.doi.org/10.3847/0004-637x/821/1/15.

Gorczyca, T.W., Kodituwakku, C.N., Korista, K.T., Zatsarinny, O., Badnell, N.R., Behar, E., Chen, M.H., Savin, D.W., 2003. Assessment of the fluorescence and auger DataBase used in plasma modeling. Astrophys. J. 592 (1), 636–643. http://dx.doi.org/10.1086/375561.

Grieken, R.E.V., Markowicz, A.A., 2002. Handbook Of X-Ray Spectrometry (Practical Spectroscopy, V. 29). Dekr.

Guerra, M., Amaro, P., Szabo, C.I., Gumberidze, A., Indelicato, P., Santos, J.P., 2013. Analysis of the charge state distribution in an ECRIS Ar plasma using high-resolution x-ray spectra. J. Phys. B: At. Mol. Opt. Phys. 46 (6), 065701. http://dx.doi.org/10.1088/0953-4075/46/6/065701.

Guerra, M., Sampaio, J.M., Madeira, T.I., Parente, F., Indelicato, P., Marques, J.P., Santos, J.P., Hoszowska, J., Dousse, J.C., Loperetti, L., Zeeshan, F., Muller, M., Unterumsberger, R., Beckhoff, B., 2015. Theoretical and experimental determination of *L*-shell decay rates, line widths, and fluorescence yields in Ge. Phys. Rev. A 92 (2), 022507. http://dx.doi.org/10.1103/PhysRevA.92.022507.

Guerra, M., Sampaio, J.M., Parente, F., Indelicato, P., Hönicke, P., Müller, M., Beckhoff, B., Marques, J.P., Santos, J.P., 2018. Theoretical and experimental determination of *K*- and *L*-shell x-ray relaxation parameters in Ni. Phys. Rev. A 97 (4), 042501. http://dx.doi.org/10.1103/PhysRevA.97.042501.

Guerra, M., Sampaio, J.M., Vília, G.R., Godinho, C.A., Pinheiro, D., Amaro, P., Marques, J.P., Machado, J., Indelicato, P., Parente, F., Santos, J.P., 2021. Fundamental parameters related to selenium Kα and Kβ emission X-ray spectra. Atoms 9 (1), 8. http://dx.doi.org/10.3390/atoms9010008.

Hubbell, J.H., Trehan, P.N., Singh, N., Chand, B., Mehta, D., Garg, M.L., Garg, R.R., Singh, S., Puri, S., 1994. A review, bibliography, and tabulation of K, L, and higher atomic shell X-Ray fluorescence yields. J. Phys. Chem. Ref. Data 23 (2), 339–364. http://dx.doi.org/10.1063/1.555955.

Indelicato, P., Desclaux, J.P., 1990. Multiconfiguration Dirac-Fock calculations of transition energies with QED corrections in three-electron ions. Phys. Rev. A 42 (9), 5139–5149. http://dx.doi.org/10.1103/PhysRevA.42.5139.

Indelicato, P., Santos, J.P., Boucard, S., Desclaux, J.-P., 2007. QED and relativistic corrections in superheavy elements. Eur. Phys. J. D 45 (1), 155–170. http://dx.doi.org/10.1140/epjd/e2007-00229-y.

Initiative, F., 2017. Roadmap document on atomic Fundamental Parameters for X-ray methodologies - version 2. URL https://www.exsa.hu/news/wp-content/uploads/IIFP_Roadmap_V2.pdf.

Kaastra, J.S., Mewe, R., 1993. X-ray emission from thin plasmas. I - Multiple auger ionisation and fluorescence processes for Be to Zn. Astron. Astrophys. Suppl. Ser. 97 (2), 443–482.

Kallman, T.R., Palmeri, P., 2007. Atomic data for x-ray astrophysics. Rev. Modern Phys. 79 (1), 79–133.

Karim, K.R., Logan, L., 1999. Theoretical lifetimes, transition rates, x-ray wavelengths, and fluorescence yields of hollow neon atoms with double k-shell vacancies. J. Quant. Spectrosc. Radiat. Transfer 61 (5), 659–664.

Kolbe, M., Beckhoff, B., Krumrey, M., Ulm, G., 2005. Thickness determination for Cu and Ni nanolayers: Comparison of completely reference-free fundamental parameter-based X-ray fluorescence analysis and X-ray reflectometry. Spectrochim. Acta B: Atom. Spectrosc. 60 (4), 505–510. http://dx.doi.org/10.1016/j.sab.2005.03.018.

Kolbe, M., Hönicke, P., Müller, M., Beckhoff, B., 2012. *L*-Subshell fluorescence yields and Coster-Kronig transition probabilities with a reliable uncertainty budget for selected high- and medium-Z elements. Phys. Rev. A 86 (4), 042512. http://dx.doi.org/10.1103/PhysRevA.86.042512.

Krause, M.O., 1979. Atomic radiative and radiationless yields for K and L shells. J. Phys. Chem. Ref. Data 8 (2), 307–327. http://dx.doi.org/10.1063/1.555594.

Krause, M.O., Oliver, J.H., 1979. Natural widths of atomic K and L levels, Kα X-ray lines and several KLL auger lines. J. Phys. Chem. Ref. Data 8 (2), 329–338. http://dx.doi.org/10.1063/1.555595.

Larkins, F.P., 1971. Dependence of fluorescence yield on atomic configuration. J. Phys. B: Atom. Mol. Phys. 4 (5), L29–L32. http://dx.doi.org/10.1088/0022-3700/4/5/001.

Liu, Y.P., Gao, C., Zeng, J.L., Yuan, J.M., Shi, J.R., 2014. Atomic data of Cu I for the investigation of element abundance. Astrophys. J. Suppl. Ser. 211 (2), 30. http://dx.doi.org/10.1088/0067-0049/211/2/30.

Löwdin, P.O., 1955. Quantum theory of many-particle systems. I. Physical interpretations by means of density matrices, natural spin-orbitals, and convergence problems in the method of configurational interaction. Phys. Rev. 97 (6), 1474–1489. http://dx.doi.org/10.1103/PhysRev.97.1474.

Marques, J.P., Sampaio, J.M., Santos, J.P., Indelicato, P., Parente, F., 2020. Theoretical fluorescence yields and widths of the K shell and the L subshells, for the Ne, Ar, and Kr isoelectronic sequences. X-Ray Spectrom. 49 (1), 69–73.

Phillips, R.W., Rehm, E.K., Henning, W., Ahmad, I., Schiffer, P.J., Glagola, B., Wang, F.T., 1987. K-shell fluorescent yields in highly stripped 57 fe atoms. J. Phys. Colloques 48 (C9), C9–311–C319–313.

Rodrigues, G.C., Indelicato, P., Santos, J.P., Patté, P., Parente, F., 2004. Systematic calculation of total atomic energies of ground state configurations. At. Data Nucl. Data Tables 86 (2), 117–233.

Sánchez Del Río, M., Brunetti, A., Golosio, B., Simionovici, A., 2003. XRAYLIB tables (X-Ray fluorescence cross-section). Eur. Synch. Radiat. Facil. Univ. Sassari 188.

Santos, J.P., Parente, F., Boucard, S., Indelicato, P., Desclaux, J.P., 2005. X-ray energies of circular transitions and electron screening in kaonic atoms. Phys. Rev. A 71 (3), 032501. http://dx.doi.org/10.1103/PhysRevA.71.032501.

Schoonjans, T., Brunetti, A., Golosio, B., Sanchez del Rio, M., Solé, V.A., Ferrero, C., Vincze, L., 2011. The xraylib library for X-ray–matter interactions. Recent developments. Spectrochim. Acta B: Atom. Spectrosc. 66 (11–12), 776–784. http://dx.doi.org/10.1016/j.sab.2011.09.011.

Smith, R.K., Brickhouse, N.S., Liedahl, D.A., Raymond, J.C., 2001. Collisional plasma models with APEC/APED: emission-line diagnostics of hydrogen-like and helium-like ions. Astrophys. J. 556 (2), L91–L95.

Tange, O., 2018. GNU Parallel 2018. Ole Tange, ISBN: 9781387509881, http://dx.doi.org/10.5281/zenodo.1146014.